Sawada et al. Appendix 2

index of contents

1. LA-ICP–MS operational settings

1.1. U–Pb dating

ICP-MS instrument	
Instrument	Nu plasma II HR-MC-ICP–MS, Nu Instruments, UK
RF power	1300 W
Detection system	Mixed Faraday-multiple ion counting array
Monitored isotopes	^{202}Hg, ^{204}Hg+^{204}Pb, ^{206}Pb, ^{207}Pb, ^{208}Pb, ^{232}Th, and ^{235}U
Detector	Three Daly detectors (D), three full size multipliers (IC) and single Faraday cup (H) IC0 for ^{208}Pb, D1 for ^{207}Pb, D2 for ^{206}Pb, IC3 for ^{204}(Hg + Pb), IC4 for ^{202}Hg, D5 for ^{235}U and H9 for ^{232}Th
Femtosecond Laser ablation system	
Instrument	Jupiter solid nebulizer
Laser wavelength	260 nm
Fluence	4 J/cm^2
Repetition rate	1000 Hz
Data acquisition time	2 s
Ablation pit size	10 μm
Carrier gas	He gas and Ar make-up gas combined outside ablation cell
He gas flow rate	0.6 L min^{-1}
Ar make-up gas flow rate	0.8 L min^{-1}

1.2. Trace-element spot analysis

ICP-MS instrument	
Instrument	iCAP TQ tandem quadrupoleICP-MS (Thermo Fisher Scientific, USA)
RF power	1550 W
Detection system	SQ-KED mode
CR gas flow rate	4 mL/min of He gas
Monitored isotopes	^{29}Si, ^{89}Y, ^{91}Zr, ^{139}La, ^{140}Ce, ^{141}Pr. ^{146}Nd, ^{147}Sm, ^{153}Eu, ^{157}Gd, ^{159}Tb, ^{163}Dy, ^{165}Ho, ^{166}Er, ^{169}Tm, ^{172}Yb, ^{175}Lu, ^{178}Hf, ^{232}Th, ^{238}U

Femtosecond Laser ablation system (spot # HGC-01-TE001~010)	
Instrument	Tandem high-spatial-resolution femtosecond laser ablation system (Fab instruments, Japan)
Laser wavelength /	260 nm
Fluence	4 J/cm^2
Repetition rate	1000 Hz
Ablation pit size	20µm × 20µm square
Carrier gas	He gas and Ar make-up gas combined outside ablation cell
He gas flow rate	0.8 L min^{-1}
Ar make-up gas flow rate	1.0 L min^{-1}

Femtosecond LA system (spot # HGC-01-TE011~017)	
Instrument	Jupiter solid nebulizer
Laser wavelength	260 nm
Fluence	4 J/cm^2
Repetition rate	1000 Hz
Ablation pit size	30µm × 30µm square
Carrier gas	He gas and Ar make-up gas combined outside ablation cell
He gas flow rate	0.6 L min^{-1}
Ar make-up gas flow rate	0.8 L min^{-1}

1.2. Trace-element imaging analysis

ICP-MS instrument	
Instrument	iCAP TQ tandem quadrupoleICP–MS (Thermo Fisher Scientific, USA)
RF power	1550 W
Detection system	SQ-KED mode
CR gas flow rate	4 mL/min of He gas
Monitored isotopes	^{57}Fe, ^{90}Zr, ^{140}Ce, ^{146}Nd, ^{157}Gd ^{172}Yb, ^{178}Hf, ^{232}Th, ^{238}U

Femtosecond LA system	
Instrument	Tandem high-spatial-resolution femtosecond laser ablation system (Fab instruments, Japan)
Laser wavelength /	260 nm
Fluence	4 J/cm^2
Repetition rate	1000 Hz
Ablation pit size	100µm × 100µm square
Carrier gas	He gas and Ar make-up gas combined outside ablation cell
He gas flow rate	0.8 L min^{-1}
Ar make-up gas flow rate	1.0 L min^{-1}

2. Analytical results of secondary reference materials for U-Pb dating

All figures in this section were generated using IsoplotR [1].

2.1. OD-3 zircon [2]

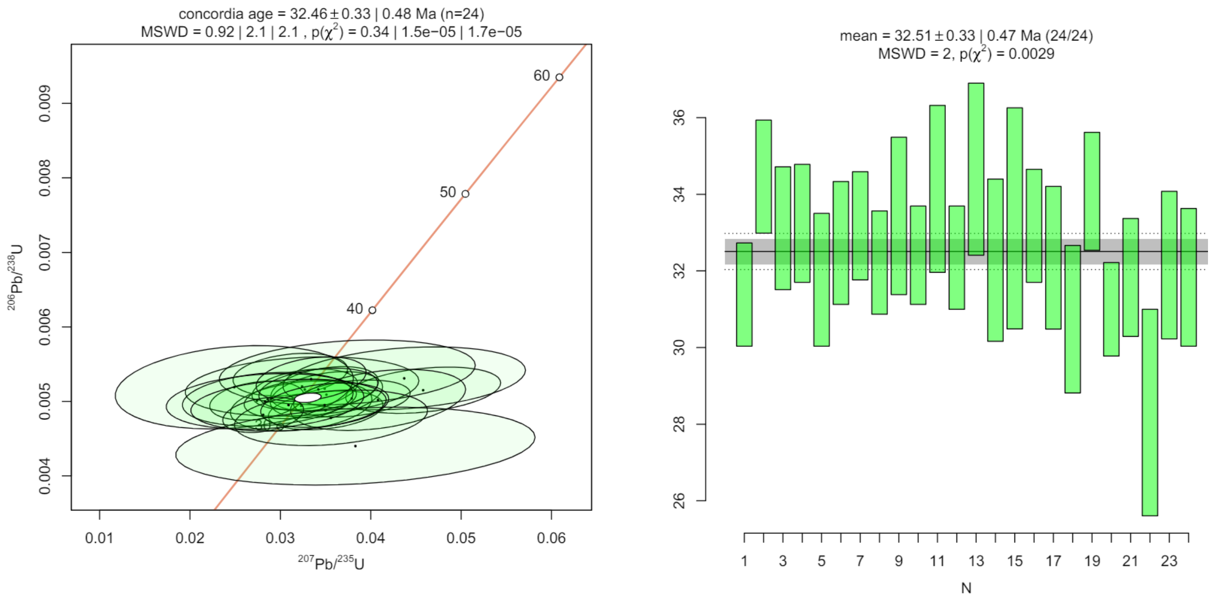

Figure A2-1. left: Wetherill plots with the calculated concordia age, right: the weighted mean of ^{238}U-^{206}Pb ages.

2.2. Kovdor baddeleyite [3,4]

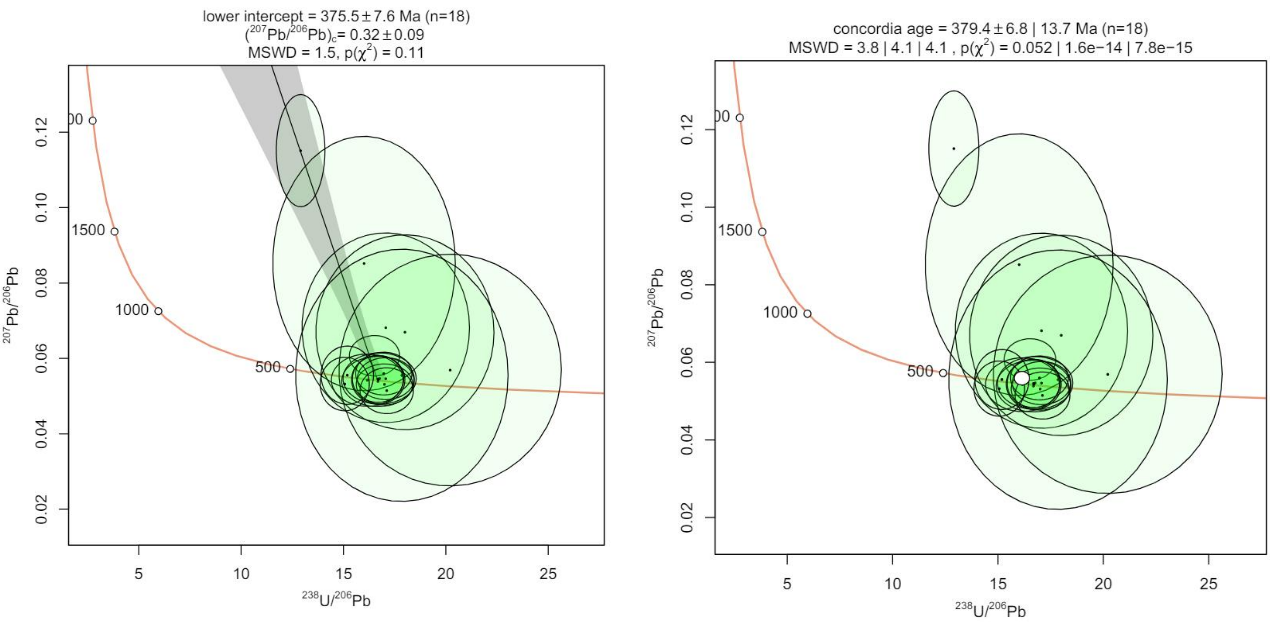

Figure A2-2 left: Tera Wasserburg plots with the calculated lower intercept age (Model-1), right: Tera Wasserburg plots with the calculated concordia age.

2.3. Phalaborwa baddeleyite [3,5]

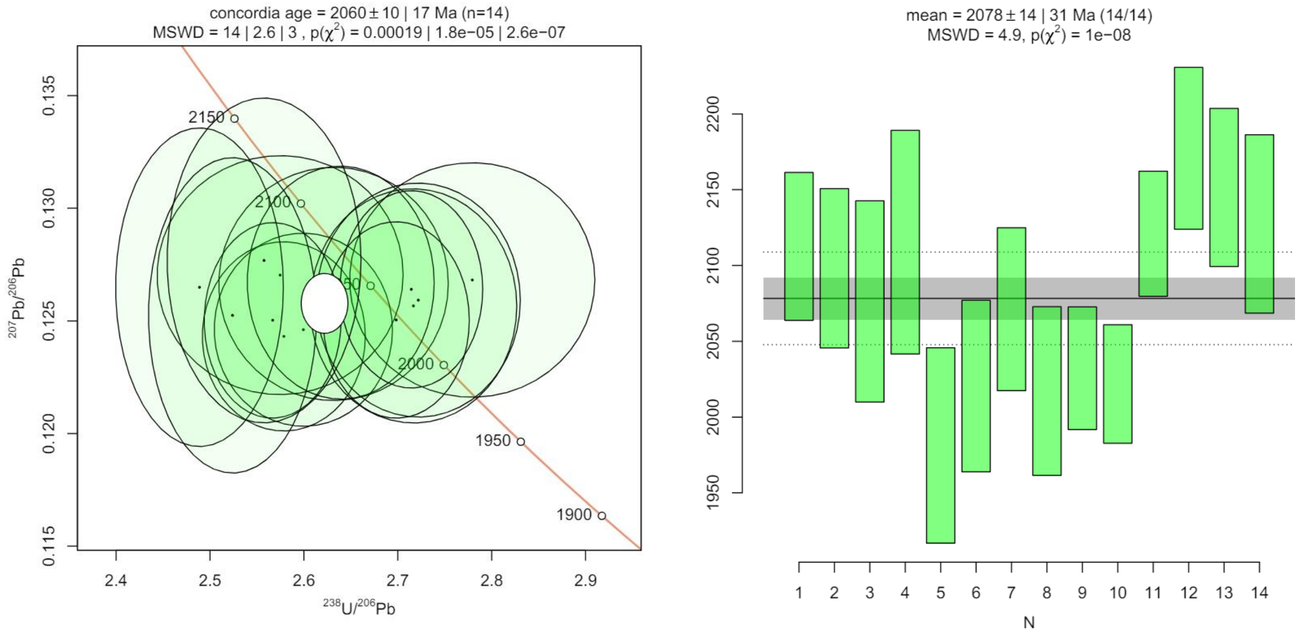

Figure A2-3 left: Tera Wasserburg plots with the calculated concordia age, right: The weighted mean of ^{238}U-^{206}Pb ages.

3. Thermodynamic calculation

Activity diagrams were constructed using equilibrium constants (Keq) calculated by the SUPCRTBL software [6]. The thermodynamic database for minerals was taken from Holland and Powell (2011) [7], and for aqueous silica from Rimstidt (1997) [8]. The activity diagram was constructed at 400 °C and 500 MPa, which corresponds to the approximate carbonation condition of Higuchi serpentinite [9]. The activity (a) of H_2O was assumed to be unity. The activity diagram shows that talc + magnesite assemblage is stable at high $a(CO_{2(aq)})$ and $a(SiO_{2(aq)})$ conditions relative to those of antigorite. Zircon is stable at high $a(SiO_{2(aq)})$, whereas baddeleyite is stable at low $a(SiO_{2(aq)})$. The boundary of the stability field of zircon and baddeleyite is at $\log a(SiO_{2(aq)}) = -2.38$ regardless of $a(CO_{2(aq)})$.

Previous study suggests that the Higuchi serpentinites undergo two steps of alteration; (i) complete serpentinization of the mantle peridotite, (ii) and subsequent carbonation of the serpentinized peridotite (Okamoto et al. 2021). The activity diagram suggests that the occurrence of zircon and baddeleyite aggregates is consistent with the history of serpentinization and carbonation. The formation of antigorite after peridotite can be simply written as

$$\underset{\text{Olivine}}{24\,Mg_2SiO_4} + 10\,\mathrm{SiO_2(aq)} + 31\mathrm{H_2O} = \underset{\text{Serpentine (antigorite)}}{\mathrm{Mg_{48}Si_{34}O_{85}(OH)_{62}}}, \quad (1)$$

which suggests that the progress of serpentinization causes the decrease in $a(SiO_2(aq))$. Therefore, zircon crystals present in the peridotite would be altered to baddeleyite when $a(SiO_2(aq))$ decreased to $10^{-2.38}$. The baddeleyite was subsequently altered to zircon in response to carbonation of the serpentine under high $a(SiO_{2(aq)})$ ($> 10^{-2.38}$) and $a(CO_{2(aq)})$.

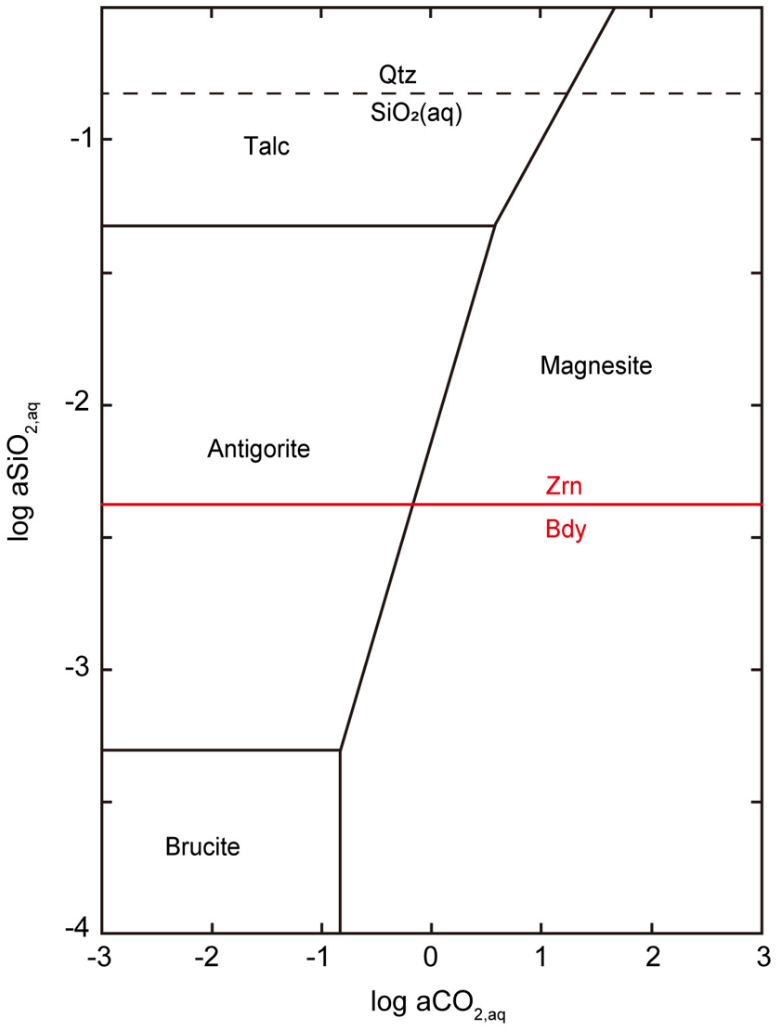

Figure A2-4 Activity diagram on the MgO-SiO_2-CO_2-H_2O system (black line) and the ZrO_4-SiO_2-CO_2 system (red line) at 400 °C and 500 MPa.

References

1. Vermeesch, P. IsoplotR: A free and open toolbox for geochronology. *Geoscience Frontiers* **9**, 1479–1493 (2018).
2. Iwano, H. *et al.* An inter-laboratory evaluation of OD-3 zircon for use as a secondary U-Pb dating standard. *Island Arc* **22**, 382–394 (2013).
3. Rodionov, N. V., Belyatsky, B. V., Antonov, A. V., Presnyakov, S. L. & Sergeev, S. A. Baddeleyite U-Pb SHRIMP II age determination as a tool for carbonatite massifs dating. *Doklady Earth Sciences* **428**, 1166–1170 (2009).
4. Li, Q.-L. *et al.* Precise U–Pb and Pb–Pb dating of Phanerozoic baddeleyite by SIMS with oxygen flooding technique. *J Anal At Spectrom* **25**, 1107 (2010).
5. Wu, F.-Y. *et al.* In situ determination of U–Pb ages and Sr–Nd–Hf isotopic constraints on the petrogenesis of

the Phalaborwa carbonatite Complex, South Africa. *Lithos* **127**, 309–322 (2011).

6. Zimmer, K. *et al.* SUPCRTBL: A revised and extended thermodynamic dataset and software package of SUPCRT92. *Comput Geosci* **90**, 97–111 (2016).
7. HOLLAND, T. J. B. & POWELL, R. An improved and extended internally consistent thermodynamic dataset for phases of petrological interest, involving a new equation of state for solids. *Journal of Metamorphic Geology* **29**, 333–383 (2011).
8. Rimstidt, J. D. Quartz solubility at low temperatures. *Geochim Cosmochim Acta* **61**, 2553–2558 (1997).
9. Okamoto, A. *et al.* Rupture of wet mantle wedge by self-promoting carbonation. *Commun Earth Environ* **2**, 151 (2021).